ASSESSMENT OF SEISMIC DAMAGE TO RAILWAY STRUCTURES USING APPLIED ELEMENT METHOD AND MICROTREMOR MEASUREMENT

Fumiaki UEHAN[1], Kimiro MEGURO[2]

SUMMARY

Methods to assess the seismic damage to railway structures were proposed in order to reduce the overall seismic damage of railway system. First, a tool for seismic performance assessment (pre-earthquake assessment) of RC structures with/without retrofit operation was developed by using the Applied Element Method (AEM). Next, a new method for quick damage inspection (post-earthquake assessment) of RC structures is proposed by using the damage judgment criteria based on the change of natural frequency and the non-contact microtremor measuring method. Besides, a plan of real-time earthquake damage assessment system (ongoing-earthquake assessment) using automatic vibration measuring devices was introduced.

INTRODUCTION

In this study, methods to assess seismic damage to railway structures are proposed in order to reduce the overall seismic damage of railway system. First, a tool for seismic performance assessment (pre-earthquake assessment) of RC structures is developed to mitigate the earthquake damage to railway. The Applied Element Method (AEM) [1], which can simulate structural behavior from elastic range to total collapse within reasonable CPU time, is applied to an assessment tool for the seismic performance of RC structures. Furthermore, a numerical model of RC column with steel jacket is developed for the retrofitted RC structures. Comparing the simulation results of cyclic loading test with seismic response of RC structures, the accuracy of the AEM is confirmed. As an application example, the optimum retrofitting method of an existing railway viaduct is determined. Next, a new method for quick damage inspection (post-earthquake assessment) of RC structures is developed for prompt restoration of earthquake-damaged railway. By using the AEM, criteria for damage judgment can be established based on the change of natural frequency of structures due to damage. The vibration characteristics of damaged structures are investigated by using a non-contact microtremor measurement method to apply an improved Laser Doppler Velocimeter. Besides, a plan of real-time earthquake damage detection system (ongoing-earthquake assessment) by using an automatic system for microtremor measurement and data transmission

---

[1] Associate senior researcher, Structural Mechanics Laboratory, Railway Technical Research Institute, Japan, E-mail: uehan@rtri.or.jp

[2] Associate Professor, International Center for Urban Safety Engineering, Institute of Industrial Science, University of Tokyo, Japan, E-mail: meguro@iis.u-tokyo.ac.jp

is introduced. Lastly, the authors discussed the application for the proposed assessment methods of pre-, ongoing and post-earthquake to the overall earthquake disaster management of railway systems.

NUMERICAL SIMULATION OF THE FAILURE MECHANISM OF RC STRUCTURES

Numerical Simulation for Earthquake Disaster Mitigation of RC Structures
It is indispensable to correctly detect weak points of RC structures and provide effective and economical reinforcement for earthquake disaster mitigation of railways in the future. In this section, we study the applicability of the AEM as an evaluation tool for the seismic performance of RC structures with and without seismic strengthening. First, the main reinforcement cutoff is considered as a weak point of RC column. For this, the change in the failure mode of RC column due to the change in the anchorage length of the main reinforcement is simulated. Then, simulations to verify the effect of the seismic strengthening of RC columns with steel jacket are carried out. Finally, in order to check whether the weak point of structure can be detected correctly by the AEM or not, the seismic response simulation of two-story RC rigid frame viaduct which collapsed during the 1995 Kobe earthquake is performed.

Numerical Simulation Technique
Figure 1 illustrates the modeling of a RC structure in the AEM. It is assumed that the structure is modeled as an assembly of small rectangular elements obtained by virtually dividing the structure. Each element is connected by pairs of normal and shear springs located at contact points, which are distributed along the element edges. In the case of two-dimensional analysis, each element has three degree of freedoms. A concrete material model is applied to each spring. At the rebar locations, two pairs of springs are used, one for the concrete and the other for the reinforcing bar. Nonlinear material models of steel and concrete as shown in Fig. 2 are given to the springs. If the spring stress exceeds its resistance, it yields and eventually fails. In this way, the AEM can follow the structural behavior from the elastic range to the total collapse.
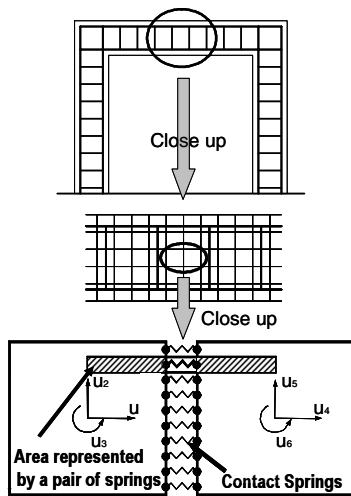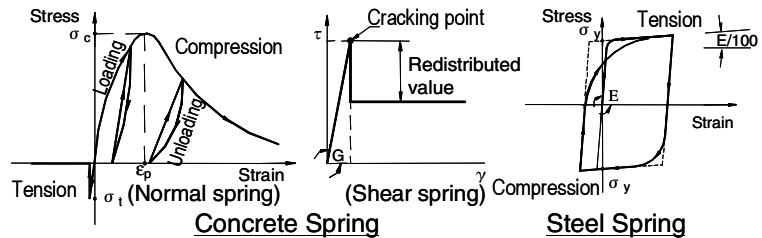

Figure 2: Material model of concrete and reinforcement

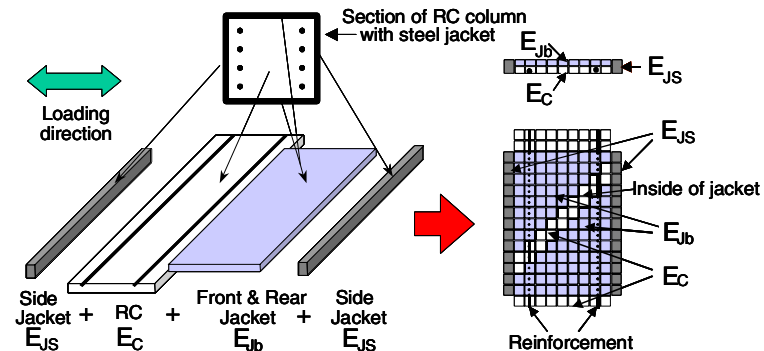**Figure 1: Modeling of RC structure in the AEM**

Figure 3: Modeling of RC column with steel jacket

The two-dimensional model of a steel jacketed column [2] is composed of three different types of elements as shown in Fig. 3. The first one is the element for the RC column inside jacket (E_C), the second one is the element for the steel jacket on the sides of the RC column (E_{JS}) and the third one is the element for the front and rear steel jacket (E_{Jb}). The first element type has RC material properties whereas the remaining have steel material properties. There is no connection between the E_{Jb} and E_C elements as shown in Fig. 3. Because the edge elements of both E_C and E_{Jb} are connected with E_{JS}, the steel jacket can restrain the inner concrete core. The concrete core may crack and the reinforcement may yield and cut.

Experiment and Numerical Simulation of Vulnerable RC Column
Outline of the Experiment and Numerical Simulation
Kawashima *et al.* [3] conducted a loading test using RC column specimens with main reinforcements having inadequate anchorage length. The details of the specimens are shown in Table 1. The difference among the four specimens is the reinforcement cutoff position. From the design viewpoint, the reinforcement development length – according to the design standard – is 116cm. The main reinforcement in Specimen n-1 is not cut, i.e. it extends along the whole column height. Half of the main reinforcement of Specimens n-2, n-3, and n-4 is cutoff at the column mid-height. In Specimen n-2, the main reinforcement length is 110cm or 6cm shorter than the recommended by the design standard whereas in Specimens n-3 and n-4, the lengths are 135cm and 160cm, respectively, longer than the design standard recommendation.
The specimen footing is fixed to the reaction floor and the cyclic load is applied to the top end by a dynamic actuator. In this case, no axial force is applied. The yield displacement δ_0 (=1.3cm) of the Specimen n-1 is defined as the standard displacement. The displacement amplitudes are gradually increased, $n \cdot \delta_0$ (n=1, 2, 3,…). The number of loading cycles per one loading step is ten. The specimens are modeled in 2-D using 620 5cm-side square elements. Plane stress condition is assumed. The strength of concrete and steel bars in the numerical model is the same as the strength of real specimens. Although the experimental loading conditions are adopted in the numerical analysis, the number of loading cycles per one loading step is one.

Table 1: Details of specimens

Specimen No.	n-1	n-2	n-3	n-4
Dimension of cross section (cm)	50×50			
Effective height (cm)	250			
Shear span ratio	5.4			
Cutoff length from base (cm)	-	110	135	160
Yield stress: main reinforcement (MPa)	308			
Yield stress: hoop reinforcement (MPa)	272			
Young's modulus: reinforcement (GPa)	200			
Compressive strength: concrete (MPa)	31.3	32.0	32.5	31.9
Young's modulus: concrete (GPa)	28.0			

Results and Considerations
Table 2 shows the maximum load for the experiment and numerical simulation. The results of numerical simulation are 90 to 97% of the experimental results. The maximum strength of the main reinforcement in the numerical simulation was assumed 1.75 times of the yield strength of the real reinforcements. It is considered that the maximum strength of reinforcement used in the simulation was smaller than the actual value.
The results of the experiment and numerical simulation are compared. Figure 4 shows the specimen failure modes and Fig. 5 shows the distribution of the main reinforcement axial strain.

Specimen n-1 (No cutoff): In both the experiment and simulation, the damage to the RC column concentrates at the column bottom. The column reinforcement fractures and the column reaches its ultimate state at displacements equal to $8\delta_0$ and $9\delta_0$ in the experiment and simulation, respectively.

Specimen n-2 (Cutoff length: 110cm): In both the cases, the damage concentrates at the center of the column where the main reinforcement is cut. The axial strain of the main reinforcement without cutoff concentrates at the end. The column reaches its ultimate state for an input displacement of $6.5\delta_0$ in the experiment and $6\delta_0$ in the simulation.

Specimen n-3 (Cutoff length: 135cm): In both cases, the damage to the RC column concentrates at the column bottom but the reinforcement cutoff region is also damaged. In the experiment, damage begins to concentrate at the bottom after a displacement of $6\delta_0$ and when it equals $8.5\delta_0$, the specimen reaches its ultimate state at the bottom. In the numerical model, the hoop reinforcement breaks when the input displacement is $6\delta_0$ after which the damage concentrates at the bottom.

Specimen n-4 (Cutoff length: 160cm): In both cases, the RC column damage concentrates at the column bottom. When the input displacement is $8\delta_0$, the column reaches its ultimate state due to the main reinforcement fracture.

Figure 4: Specimen layout (Upper) and failure mode (Lower: experiment (Left), simulation (Right))
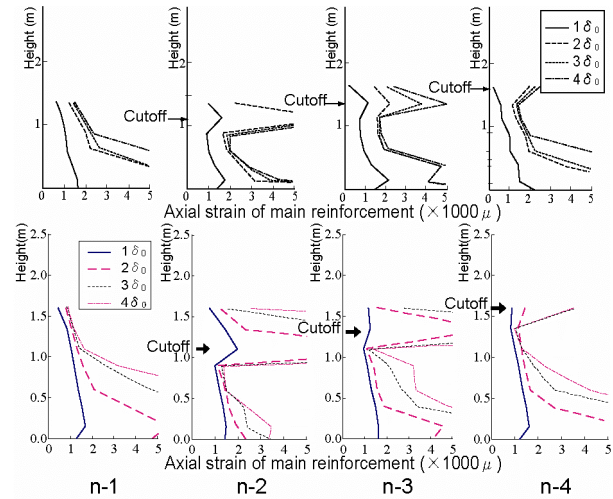
Figure 5: Main reinforcement axial strain (Upper: experiment, Lower: simulation)

In the experiment, the Specimen n-2, which has the shortest development length, is damaged at the column center where the main reinforcements are cut. As the development length increases, the damaged region shifts to the column bottom and the damage state approaches Specimen n-1, which has continuous main reinforcement. The AEM numerical simulation results followed well the phenomenon that occurred in the experiments. The maximum strength and ultimate displacement obtained with the simulation coincided with the experimental results. The simulated axial strain of the main reinforcement fairly agrees with the experiment results, and the simulated results followed the tendency of the strain distribution changes that accompany the changes of the development lengths. It is well known that the measurement of the reinforcement strain is very difficult in case of damaged RC structures. Kawashima *et al.* [3] pointed out that a certain error might be included in the axial strain experiment results. Therefore an extensive discussion of the accuracy of the simulated strain is not considered necessary
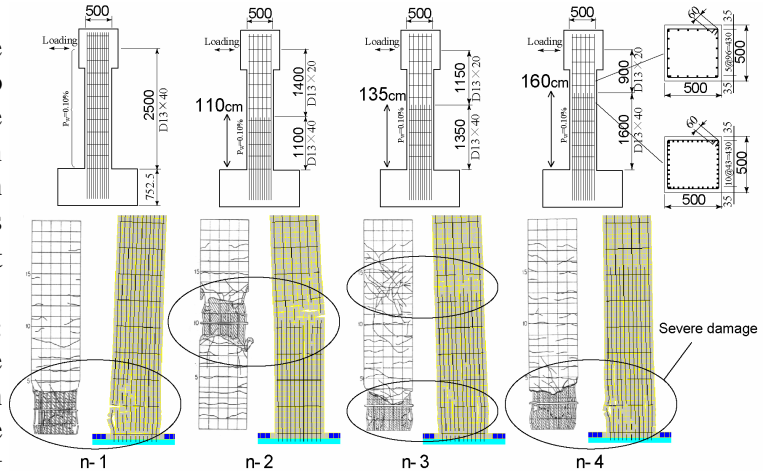
Table 2: Comparison of maximum strength

Specimen No.	n-1	n-2	n-3	n-4
Experiment (kN)	167	148	161	166
Simulation (kN)	154	143	145	160

Experiment and Numerical Simulation of RC Column Reinforced by Steel Jacket

Outline of Experiment and Numerical Simulation

In order to check the effect of earthquake strengthening of RC columns by steel jacketing, Kawashima *et al.* [3] conducted loading tests of RC specimens with steel jackets. Table 3 shows the details of the specimens used in the experiment. The details of those specimens are almost the same being the difference among them the steel jacket length. The reinforcements of all specimens are cut 90cm above the base, which is 22cm shorter than the design standard recommendation. Specimen j-1 is not strengthened. The steel jacket of Specimen j-2 is 50cm long and the center of the steel jacket coincides with the main reinforcement cutoff level. A 75cm-long steel jacket is used for Specimen j-3 and the main reinforcement cutoff level is 25cm above the jacket lower edge. The tensile strength of steel jacket is 274MPa and the space between the RC column and the steel jacket is filled with a 3mm-thick epoxy resin. The boundary and loading conditions of this set of experiments are similar to those of the experiments described in the previous section. However, in this case 282kN of axial force is applied and the failure displacement δ_0 (=1.5cm) of the Specimen j-1 is defined as the standard displacement. Each specimen is modeled in 2-D with 640 5cm-side square elements. Plane stress condition is assumed. The strength of concrete and steel bars of numerical models is same as the strength of real specimens. Although the experimental loading conditions are adopted in the numerical analysis, the number of loading cycles per one loading step is one.

Table 3: Details of specimens

Specimen No.	j-1	j-2	j-3	(j-4)
Dimension of cross section (cm)	50×50			
Effective height (cm)	260			
Shear span ratio	5.6			
Cutoff length from base (cm)	90			
Yield stress: main reinforcement (MPa)	409	357		
Yield stress: hoop reinforcement (MPa)	433	245		
Thickness: steel jacket (cm)	-	1.0		
Length: steel jacket (cm)	-	50	75	30
Young's modulus: reinforcement (GPa)	200			
Compressive strength: concrete (MPa)	42.0	43.8	35.6	35.6
Young's modulus: concrete (GPa)	28.0			

Results and Considerations

Table 4 shows the maximum load obtained experimentally and numerically. The numerical simulation results are 100 to 105% of the experiment results. Figure 6 shows the observed failure modes and Fig. 7 shows the distribution of the main reinforcement axial strain obtained by the experiment and simulation.

Specimen j-1 (Without jacketing): In the both experiment and simulation, the damage to the RC column concentrates at the end. The RC column reached its ultimate state for a displacement equal to $7\delta_0$ in the experiment and $6\delta_0$ in the simulation.

Specimen j-2 (Steel jacket length: 50cm): The column center near the upper end of the steel jacket and the column bottom were damaged in the experiment and simulation. Finally, the bottom end damage became severe.

Specimen j-3 (Steel jacket length: 75cm): In both experiment and simulation, the RC column damage concentrates at the column bottom. The RC column reached its ultimate state when the input displacement was $7\delta_0$ in the experiment and $6\delta_0$ in the simulation.

Specimen j-4 (Steel jacket length: 30cm - Only numerical simulation): A RC column strengthened with a 30cm-long steel jacket was simulated in order to check the failure mode of a vulnerable column with inappropriate jacketing. In this case, the damage concentrated at the column section near the upper end of the steel jacket.
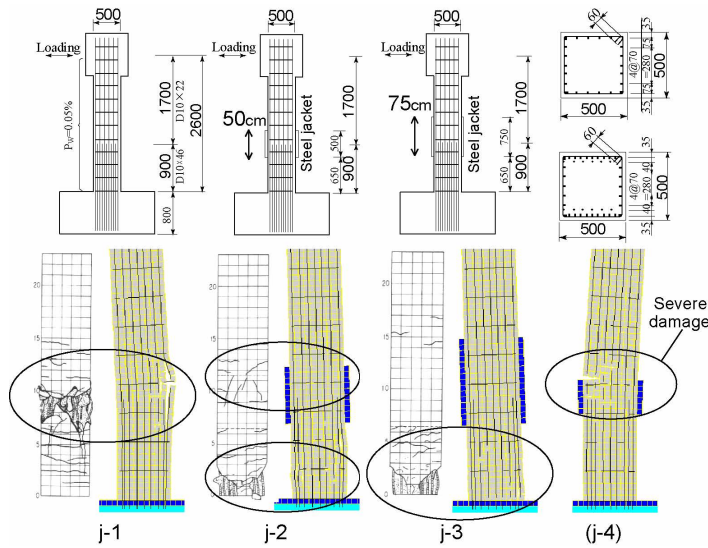
**Figure 6: Specimen layout (Upper) and failure mode
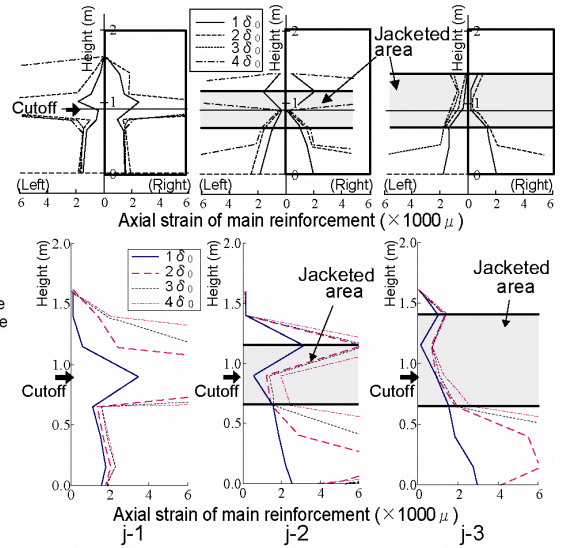(Lower: experiment (Left), simulation (Right))**

**Figure 7: Main reinforcement axial strain
(Upper: experiment, Lower: simulation)**

In the experiment, we confirmed that the damage of the Specimen j-1, which is not strengthened, concentrates at the column center where the main reinforcement is cut and the region where damage concentrates shifts to the lower part of the column as the steel jacket length increases.

The results of the numerical simulation by AEM showed the same phenomenon that occurred in the experiments. The maximum strength and ultimate displacement were simulated with sufficient accuracy. Moreover, the simulated failure mode results of the Specimen j-4 suggest that numerical simulation by AEM may be effectively utilizable as the detection method of inadequate earthquake strengthening design.

Table 4: Comparison of maximum strength

Specimen No.	j-1	j-2	j-3
Experiment (kN)	124	128	126
Simulation (kN)	127	129	133

Simulation of Collapse Behavior of Real Viaduct

Numerical simulation of the seismic response of the Japan Railways (JR) Hansui viaduct, which was collapsed due to the 1995 Kobe Earthquake, is performed. The damage condition [4] is shown in Fig. 8. The structure is a 3-span double-decked viaduct with a typical section as shown in Figure 9. 18cm-side square elements are used to model the viaduct. The number of distributed springs between each two adjacent sides is 10. The material properties of concrete and steel bars are defined by considering the actual strength as showed in Table 5. The arrangement of reinforcing bars is the same as the real arrangement shown in Fig. 9. The natural frequency of the numerical model considering the effect of the soil-pile system is almost the same as the real natural frequency of the undamaged Hansui viaduct. The collapse behavior of the model due to the NS component of the JR Takatori ground motion [5] is shown in Figure 10. The damage condition of the numerical model is almost the same as the observed one.

Table 5: Material properties of viaduct model

Concrete		Reinforcing bar	
Young's modulus (GPa)	28.0	Young's modulus (GPa)	210
Compressive strength (MPa)	32.0	Yield stress (MPa)	350
Tensile strength (MPa)	2.40		

Application to Selection of Optimum Retrofitting Method

One of the important features of the AEM is that it can follow material nonlinearity of structure form the early stage of loading till the occurrence of total collapse. The method presents useful tool to predict the damage mechanism and ultimate behavior of structures during the severe earthquakes.
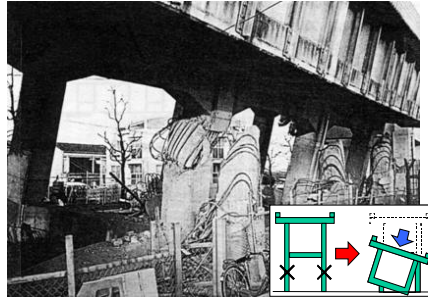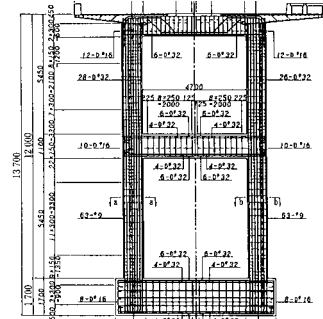
In this section, three different seismic retrofitting methods for the railway viaduct (shown in Fig. 11) were examined to select optimum retrofitting method. The static push-over analysis had been performed four different viaducts models shown in Fig.12 which shows the damage conditions for the models based on AEM analysis. The relations between load and displacement (P-δ curve) are shown in Fig. 13. Several observations can be illustrated as followed:

The middle beam of Model A (system without retrofitting) was destroyed first then the lower columns were destroyed. Model B showed the worst performance since the collapse had been occurred at the early stage due to the shear failure of the lower columns. Therefore, the retrofitting method applied to the model B seems to be unsuitable as a countermeasure of the very severe earthquake such as Level 2 earthquakes defined in Japan (L2). Even the middle beam of Model C was destroyed similar to Model A, Model C did not collapse because of retrofitting of the lower columns. This retrofitting method of Model C is quite enough to prevent the viaduct collapse due to L2 earthquakes.
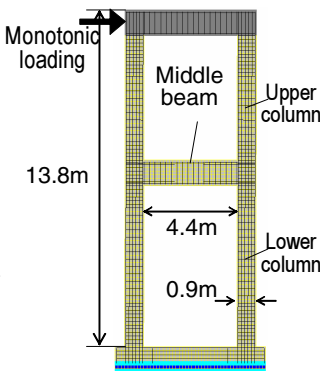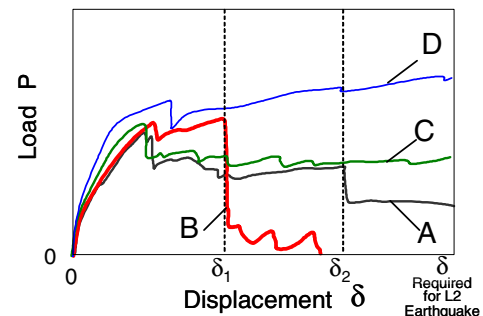

Figure 8: Damage condition of Hansui viaduct

Figure 9: Viaduct layout

Fig. 10: Collapse behavior of numerical model due to ground motion of JR Takatori site

Figure 11: Viaduct model

Figure 13: Relations between load and displacement

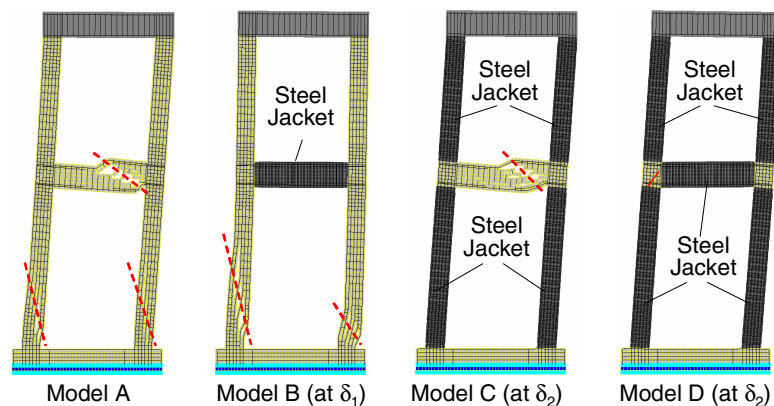Model A   Model B (at δ_1)   Model C (at δ_2)   Model D (at δ_2)

Figure 12: Damage conditions of numerical models

Finally, the retrofitting method of Model D demonstrated the best performance compared with other retrofitting models. This model is highly recommended to maintain sufficient seismic strength more than the requirements of L2 earthquakes.

SIMULATION OF THE CHANGE OF NATURAL FREQUENCY DUE TO DAMAGE

Applicability of Vibration Measurements for Damage Inspection

The degree of damage of a RC structure, especially a jacketed structure, cannot be fully grasped by visual inspection. On the other hand, the inspection techniques by using dynamic characteristic of structure have been developed in the field of health monitoring of railway structures. The inspection techniques make use of the natural frequency of structures as the index of damage and/or deterioration levels. The vibration induced by sources such as a moving train or car, impact on the structure and microtremors, is used in order to get the natural frequency of structure. In order to assess the degree of damage to a RC structure using the inspection techniques based on vibration measurements, it is necessary to identify the changes of the dynamic characteristics associated with structural damage. For example, the damage levels of RC structure are defined as shown in upper part of Fig. 14 in the field of design of railway structure. If the natural frequency corresponding to each damage level is accurately calculated by AEM, the accuracy of the inspection method is expected to be improved very much. Therefore, the accuracy of the AEM to simulate the natural frequency of damaged structures is investigated through the comparison of the experimental results and numerical simulations.

Simulation of Natural Frequency of a Damaged RC Column

Experiments to grasp the change of natural frequencies of RC columns due to damage were carried out [6]. The specimen used in the experiment, which is a scale model of railway viaduct column, is shown in Fig. 15. Cycling loading was applied to gradually damage the specimen. Impact vibration tests, in order to get the specimen natural frequency, were performed at each damage level. The specimen material properties that were obtained through material tests are shown in Table 6. The specimen was modeled with 5cm-side square elements. The number of distributed springs between two adjacent elements was 10. In case of the experiment, 1 loading step was composed of 3 cycles, and the impact vibration test was carried out after each step. The upper graph of Fig. 16 depicts the inputted displacement and lower graph shows the natural frequency changes for both experiment and simulation.

In case of the numerical simulation, the results of the case in which 1cycle/step is considered are shown in Fig. 16 because there are not major differences between 1cycle/step and 3cycles/step cases. The simulated natural frequencies of 1/4, 1/2 and 3/4 cycles are also shown in Fig. 16. The simulated results agree well with the experimental results.
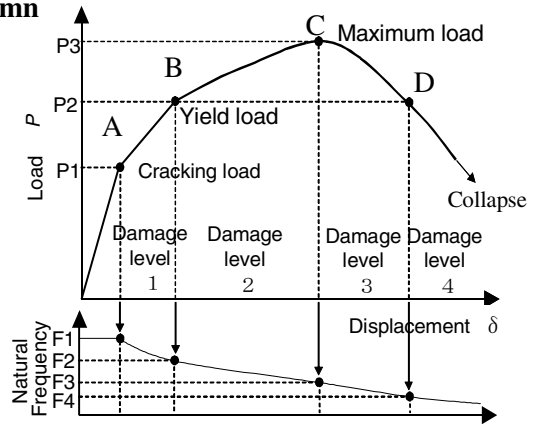
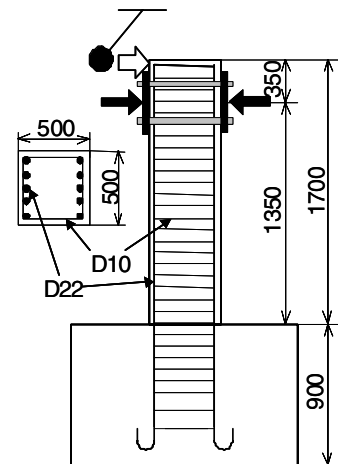**Figure 14: Definition of damage levels of RC structures**

Figure 15: Specimen used in the experiment

Table 6: Material properties of specimen

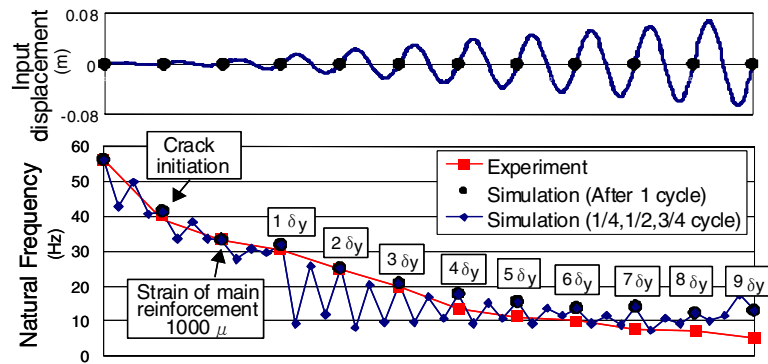| Concrete	Column	Footing
Young's modulus (GPa)	21.9	22.1
Compressive strength (MPa)	28.5	28.7
Tensile strength (MPa)	2.25	2.77
Reinforcing bar	D22	D10
Young's modulus (GPa)	193	181
Yield stress (MPa)	421	385

Figure 16 Input displacement (Upper) and change of natural frequency due to damage (Lower)
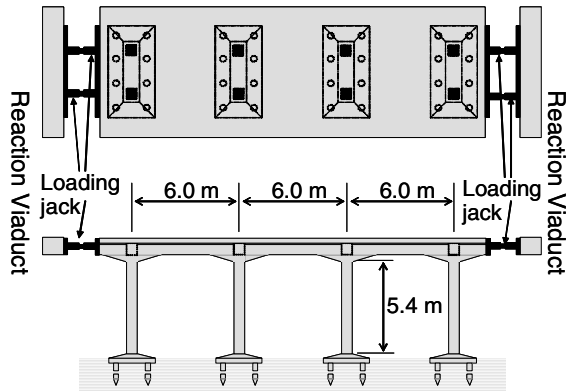

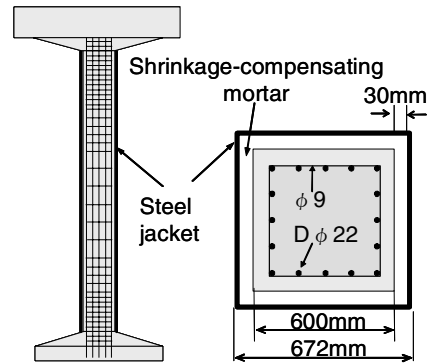**Figure 17: Viaducts and loading equipments**

Figure 18: Arrangement of reinforcing bars and cross section of the jacketed column

Simulation of the Natural Frequency of a Damaged RC Viaduct Reinforced by Steel Jacket

Outline of Experiment and Numerical Simulation

Naganawa *et al*. [7] conducted the loading experiment of a real viaduct reinforced by steel jacket. Daiichi Shinagawa viaduct R13, which was removed due to the opening of Shin-Shinagawa station, was used in the experiment. The viaduct structure is a 3-span, single lane, RC rigid frame supported with 2 columns. The typical section of the viaduct and the loading equipment are shown in Fig. 17. Each column was reinforced with a 6-mm thick steel jacket as shown in Fig. 18. The gap between the column and the steel jacket was 30mm, and it was filled with shrinkage-compensating mortar. Walls were installed in the frames adjacent to R13, namely R12 and R14, to act as reaction walls.

Figure 19: Jacketed column numerical model

The slabs between viaducts were cut and the loading jacks were installed there. The cyclic loading test along the direction parallel to the track was carried out by displacement control. After applying cyclic loadings with maximum displacements of ±15mm, ±30mm, ±60mm, ±90mm, ±120mm, ±150mm, ±180mm, ±210mm, and ± 240mm, a monotonic loading of +350mm was imposed as the last step. The impact vibration test along the direction parallel to the track was carried out after each loading step in order to investigate the natural frequency changes due to the structural damage.

The viaduct column was modeled using AEM considering 8.25cm-side square elements as shown in Fig. 19. It was assumed that the top of the column was restrained against rotation because the viaduct beam was very rigid. The behavior of the whole viaduct was represented with one column carrying one eighth
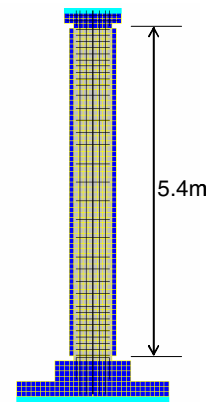
of the total mass of the slab and beams. The design compressive strength of the concrete of the viaduct was 23.5 MPa, and the compression test results, which were obtained at the time of construction, gave a compressive strength of 32.9 MPa. SD49 and SS41 were used for the longitudinal reinforcing bars and stirrups, respectively. At the first stage of the analysis, the properties of the material of the viaduct were not fixed. Six models with different material properties, as shown in Table 7, were created by combining the material properties of three types of concrete and the two types of longitudinal reinforcing bar as shown in Table 8. In addition, by arranging a soil-foundation spring at the bottom of the model, the natural frequency of the column was adjusted so that it became equal to the measured natural frequency of the real viaduct. As a result, the natural frequencies of all the models were equal in the initial state. The changes of the natural frequency of each model due to the structural damage were analyzed and compared with the experimental results.

Table 7: Combination of material properties

Case	(1)	(2)	(3)	(4)	(5)	(6)
Concrete	C1	C1	C2	C2	C3	C3
Longitudinal bars	S1	S2	S1	S2	S1	S2

Table 8: Material properties of numerical model

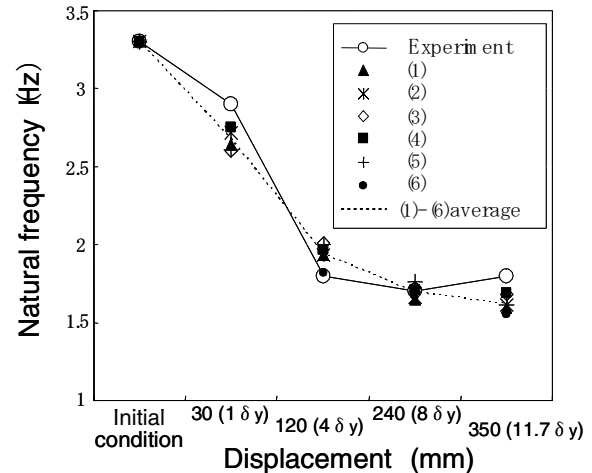|	Compressive strength (MPa)	Young's modulus (GPa)		Yield stress (MPa)	Young's modulus (GPa)
C1	23.5	24.5	S1	490	200
C2	35.0	28.0	S2	558	200
C3	17.6	21.6	Stirrup	400	200

Figure 20: Change of natural frequency of the real viaduct and the numerical models

Results and Considerations
The experimental and numerical results are shown in Fig. 20. According to the experimental results, the natural frequency reduced to 85% of the original value after the ±30 mm loading. After the ±120mm loading, the natural frequency reduced to 50% and it remained almost constant after that. In the simulation result by AEM, the natural frequency reduced to 79 - 83% after the ±30mm loading, to 55 - 61% after the ±120mm loading, to 50 - 54% after the ±240mm loading, and to 47 - 51% after the +350mm loading. In the numerical simulation results, the difference of the material properties of each model did not have much influence on the natural-frequency change.

EFFECTIVE VIBRATION MEASURING METHOD OF RAILWAY STRUCTURE

Development of Non-contact Microtremor Measuring Method
Non-contact Microtremor Measuring Method
In this section, an accurate non-contact measuring method for structure microtremor is proposed by using the improved Laser Doppler Velocimeter (LDV).
As previously mentioned, in the field of health monitoring of railway structures, the vibration induced by various sources is used to determine the natural frequency of structures. Microtremors are very small ground vibration under normal conditions due to natural and artificial sources, such as tidal waves, traffic noise, industrial vibration and so on.   Microtremor measurement is one of the most efficient and safest methods for the purpose because no special vibration sources like a moving car or impact by hitting structures is necessary. By microtremor measurement, the dynamic characteristic of a structure such as the natural frequency can easily be obtained.

Furthermore, the following advantages are obtained by developing a non-contact microtremor measuring method. The first advantage is the improvement of the efficiency of vibration measurement work by omitting the installation and removal of sensors and cables (Fig. 21). The second advantage is the improvement of the safety of vibration measurement work. In the inspection of railway structures such as viaducts or bridges, sensors might be installed at dangerously high places. In the case of earthquake damage inspection, inspection engineers are exposed to the risk of secondary disaster due to aftershocks. Sensors need not be installed at dangerous positions on structures when the non-contact measuring method is adopted (Fig. 21).

The authors decided to use the Laser Doppler Velocimeter (LDV) for the non-contact microtremor measuring method. LDV is an optical measurement device that is able to detect the velocity of moving objective by using the difference in frequency between incident and reflected lasers (Fig. 22). A method is proposed below to solve the problems related to microtremor measurement by using LDV. The accuracy of the measuring method is verified by the results of non-contact measurement of an existing reinforced concrete structure.

Problems of Microtremor Measurement by Using LDV

LDV is a device that detects the relative velocity between LDV itself and the measuring object. Therefore, the vibration of LDV itself has a significant influence on the measurement record, when a very small vibration is measured. In the case of the outdoor microtremor measurement of railway structures, the vibration of the LDV itself, which is caused by various ground vibrations and/or winds, can not be disregarded (Fig.23). The influence of LDV vibration is especially serious in the case of the damage inspection after an earthquake, because it is executed under a high noise condition due to restoration work. Therefore, a method that can remove the influence of LDV vibration is indispensable for highly accurate measurement of structure microtremors.
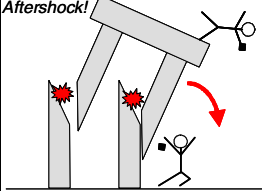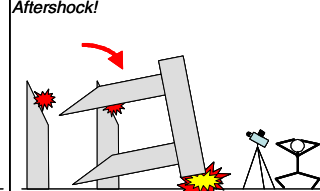

Figure 21: Advantages of non-contact measurement

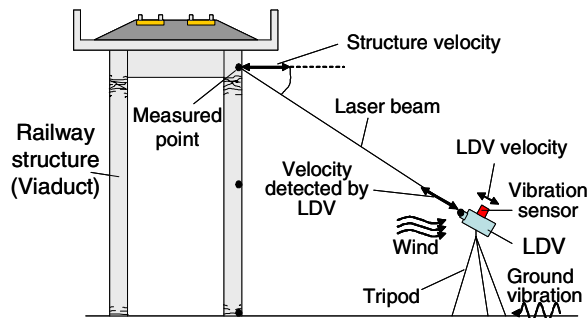**Figure 22: Laser Doppler Velocimeter (Graphtec: AT0023)**

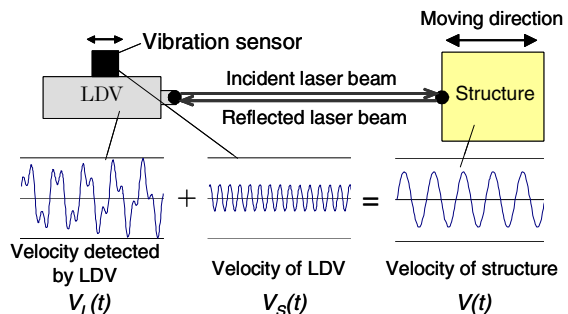**Figure 23: Outline of non-contact microtremor measurement**

Figure 24: Removal of influence of LDV vibration

Method to Remove the Influence of LDV Vibration

The authors developed a method to remove the influence of LDV vibration by using the record of the vibration sensor installed in LDV (Fig. 24). The velocity $V_L(t)$ of LDV at time t is a relative velocity between the measured point on the structure and LDV. The $V_S(t)$ is the velocity of LDV recorded by the vibration sensor installed in LDV at time t. Then, the absolute velocity of the measured point $V(t)$ from which the influence of LDV vibration is removed is shown by the next equation.

$$V(t) = V_L(t) + V_S(t) \qquad (1)$$

When the angle of the direction of laser irradiation and movement of structure is θ, the absolute velocity of the measured point $V(t)$ is shown by the next equation [8].

$$V(t) = (V_L(t) + V_S(t)) / \cos\theta \qquad (2)$$

Identification of Dynamic Characteristics of Real RC Structure

The first mode natural frequency and mode shape of an existing RC structure shown in Fig. 25 were identified by using the proposed non-contact microtremor measuring method. The microtremors of the structure from the point A to E were sequentially measured by an improved LDV that has a vibration sensor and telephoto lens (Fig. 26) installed 5.2m away from the structure as shown in Fig. 25. When each point was measured, microtremors at the LDV and the point R of the structure were measured by vibration sensors simultaneously.

Fig. 27 shows the record of each sensor obtained when the point A was measured. The vibration of the point A identified by the proposed method is also shown in Fig. 27. Fig. 28 shows the Fourier spectrum of the waves shown in Fig. 27. Although the data recorded by the LDV with no correction was strongly influenced by LDV vibration, the results identified by the proposed method almost correspond to the real structure microtremor recorded at the point R.

Next, the first mode shape of the lower column of the structure was estimated. The spectrum amplitude of 3.6Hz at the point A to E was standardized by those obtained by the simultaneous measurement at the point R. The standardized spectrum amplitude is considered to be the mode amplitude of the column. The estimated mode shape was shown in Fig. 29. The result estimated by the proposed method was corresponding to the mode shape obtained by the numerical analysis.
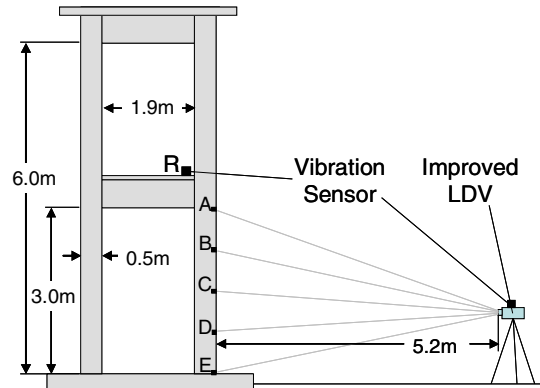

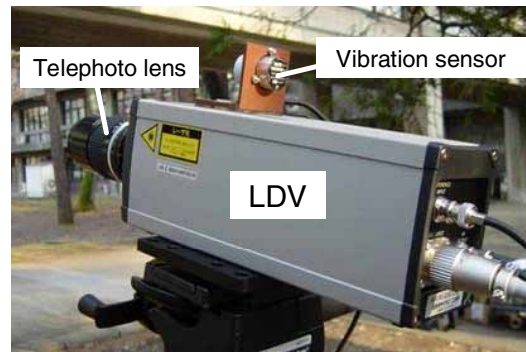**Figure 25: Outline of measurement and measured RC structure**
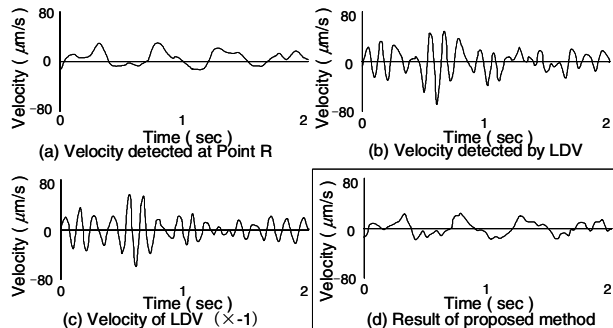

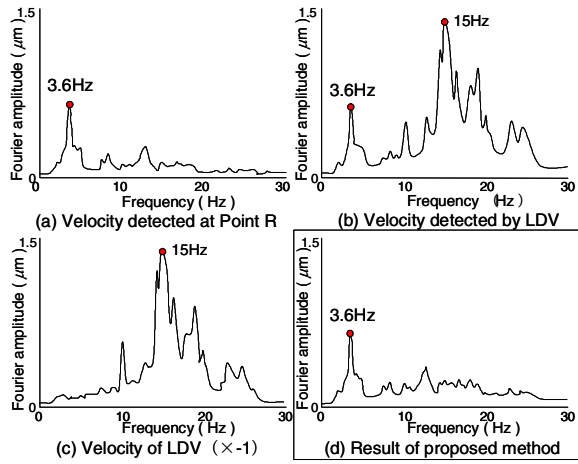**Figure 26: Improved LDV**

Figure 27: Velocity at measured points

Figure 28: Fourier spectra at measured points

(a) Velocity detected at Point R
(b) Velocity detected by LDV
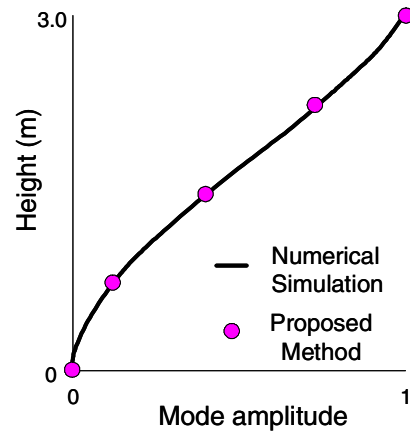(c) Velocity of LDV (×-1)
(d) Result of proposed method

Figure 29: Fundamental mode shape
of RC column

From these results, the proposed non-contact microtremor measuring method is considered to be a good tool for the inspection of railway structures as sufficient accuracy.

Development of Automatic Vibration Monitoring System
Automatic Vibration Monitoring System
In order to expand the application area of the vibration diagnosis of structure, an automatic vibration monitoring system was developed. An outline and specifications of the system are shown in Fig. 30 and Table 9, respectively.

Table 9: Specifications of the automatic vibration measuring system

Size	Main body: 0.4:0.4:0.2m, Solar panel: 0.5m^2, Wind generator: ϕ0.5m
Measuring object	Acceleration (Microtremor & Strong motion)
A/D converter	6ch, 24bit
Sensor	Accelerometer (JAE-2G: 6ch)
A/D controller	Trigger control & Timer control
Data transmission	PHS (Trigger & Timer transmission)
Memory	Data memory: 40kWord, Delay memory: 8kWord
CPU	Libretto L1/060TNMM, (CPU: Crusoe TM5600 600MHz, Hard disk 10 GB)
Power supply	DC12V, Solar panel (48W), Wind generator (25W), Battery (80W)
Power controller	2 way parallel charge, Automatic cutoff: 11.5V, Automatic restart: 12.6V

Because of the compact size and the natural energy drive, the automatic measuring device can be installed in various structures. When battery energy is insufficient due to the lasting of calm rainy days, the system automatically stops monitoring. It automatically restarts when the battery is recharged by natural sources. The prototype system has been working without maintenance for more than one year and succeeded in continuous monitoring for 60 straight days.
This system has the function of remote monitoring of structures. The timer control function is used for health monitoring of a structure by means of long-term monitoring of natural frequency. The trigger control function is used to detect emergencies such as earthquakes, freshets, collisions, and construction accidents.

Application to Real-time Damage Detection for the Railway System
The automatic monitoring system can be used as a real-time damage detection system. The system can monitor the ground motion and structural response due to earthquakes by triggering control function. The data of the changes in the natural frequency is processed and transmitted to the center system. The detected structural damage is displayed as shown in Fig. 31. Unlike the conventional damage prediction system, this proposed system can detect actual seismic damage of structures. This system is expected to contribute to early warning, downtime reduction, evacuation guidance, early setting up of emergency task force and so on.
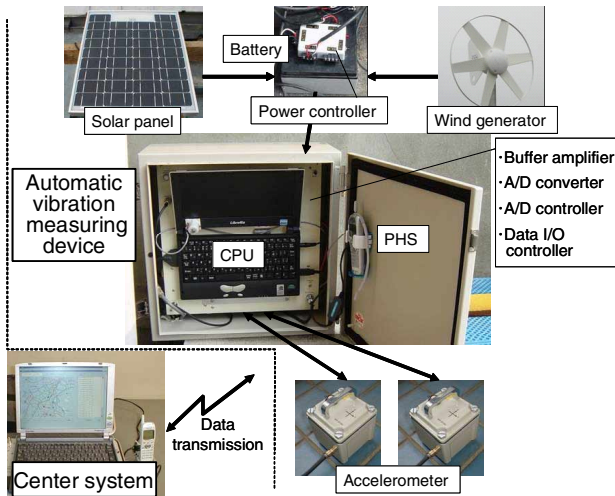

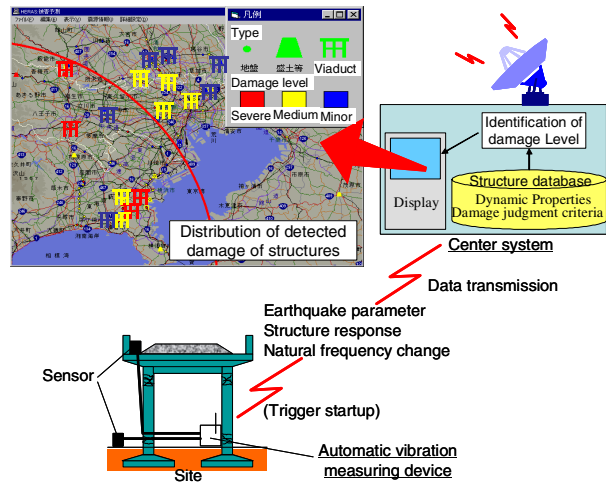**Figure30 Outline of automatic vibration monitoring system**

Figure 31: Outline of real-time damage detection system.

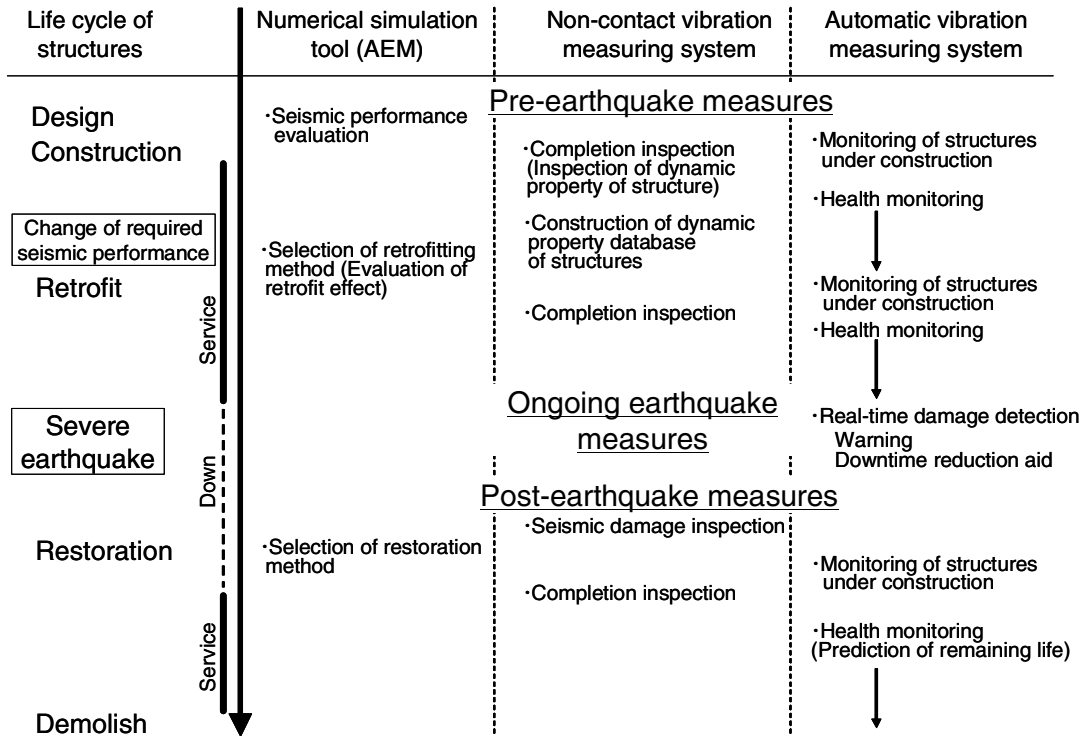| Life cycle of structures	Numerical simulation tool (AEM)	Non-contact vibration measuring system	Automatic vibration measuring system
Design Construction	·Seismic performance evaluation	Pre-earthquake measures	
		·Completion inspection (Inspection of dynamic property of structure)	·Monitoring of structures under construction
			·Health monitoring
Change of required seismic performance		·Construction of dynamic property database of structures	
Retrofit	·Selection of retrofitting method (Evaluation of retrofit effect)		·Monitoring of structures under construction
		·Completion inspection	·Health monitoring
Severe earthquake		Ongoing earthquake measures	·Real-time damage detection Warning Downtime reduction aid
		Post-earthquake measures	
Restoration	·Selection of restoration method	·Seismic damage inspection	·Monitoring of structures under construction
		·Completion inspection	·Health monitoring (Prediction of remaining life)
Demolish			

Figure 32: Concept of overall damage assessment of structure

CONCLUSIONS

In this study, effective tools are developed to assess the earthquake damage of railway structures. A numerical simulation tool to apply AEM is used for seismic performance evaluation for RC structures with/without retrofit operation. Furthermore, the numerical simulation tool is used to establish damage judgment criteria for vibration diagnosis. The non-contact microtremor measuring system is useful for microtremor measurement in the vibration diagnosis of structures. The automatic vibration monitoring system is useful for structural health monitoring, and can be used as a real-time damage detection system of railway systems. Fig. 32 shows the relation between the developed tools and the seismic damage assessment work in the structure life span. If these tools are effectively used, the overall (pre-, ongoing and post-earthquake) damage assessment of railway structures is realized.

REFERENCES

1. Meguro, K. and Tagel-Din, H., "A new efficient technique for fracture analysis of structures," Bulletin of Earthquake Resistant Structure Research Center, IIS, Univ. of Tokyo, No.30, 1997, 103-116.
2. Uehan, F. and Meguro, K., "Vulnerability assessment of jacketed viaduct using microtremor measurement & numerical simulation," Proceedings of 12th World Conference of Earthquake Engineering (CD-ROM), 2000.
3. Kawashima, K., Unjoh, A., and Iida, H., "Seismic inspection and seismic strengthening methods of reinforced concrete bridge piers at mid-height where main reinforcements are terminated with inadequate anchorage length," Report of Public Works Research Institute Ministry of Construction, Vol. 189, 1993 (in Japanese).
4. Editorial committee for the report on the Hanshin-Awaji earthquake disaster, "Report on the Hanshin-Awaji earthquake disaster, Damage to civil engineering structures, Bridge structure," Maruzen, 1996.
5. Nakamura, Y., Uehan, F. and Inoue, H., "Waveform and its analysis of the 1995 Hyogo-Ken-Nanbu earthquake II," JR earthquake information, No. 23d, RTRI, 1996, 9-16.
6. Shimono, H., Watanabe, T. and Sato T., "A consideration on the damage evaluation of RC members," Proceedings of the 52th annual conference of the Japan Society of Civil Engineering I-A, 1997, 402-403 (in Japanese).
7. Naganawa, T., Tanma, Y., Yoshida, K., Kaji, K. and Nakano, S., Experimental study on real RC frame viaduct reinforced by steel (Vol. 2) –Study on soundness diagnosis of RC frame viaduct reinforced by steel after earthquake-," *Proceedings of 55th annual conference of JSCE*, V-501, 2000, 1004-1005 (in Japanese).
8. Uehan, F. and Meguro, K., "Development of non-contact microtremor measuring method for vibration diagnoses of railway structures," JSCE Journal of Earthquake Engineering, Vol. 27 (CD-ROM), 2003 (in Japanese).